AIAA-94-1875-CP

SOME ASPECTS OF THREE DIMENSIONAL SUPERSONIC/HYPERSONIC INVISCID BLUNT BODY FLOW COMPUTATIONS EMPLOYING HIGH RESOLUTION TVD SCHEMES BASED ON ROE'S RIEMANN SOLVER

S. K. Saxena * and K. Ravi †

Computational and Theoretical Fluid Dynamics Division
National Aerospace Laboratories
Bangalore, India

Abstract

This paper discusses some aspects of three dimensional supersonic and hypersonic inviscid blunt body flow computations. The method is based on the solution of the Euler equations employing an explicit, upwind TVD (MUSCL) formulation of the Roe Riemann Solver within the cell centered finite volume approach. A comparative study of various limiters and entropy fixes is carried out to identify the most appropriate combination. The effect of using cell spacing in the TVD extrapolations is highlighted. Local time stepping and code parallelization has been employed to accelerate convergence in terms of effective wall clock times.

Nomenclature

$\mathbf{A}$	flux Jacobian
C_p	pressure coefficient
$\hat{\mathbf{E}}$	transformed flux vector
$\hat{\mathbf{F}}, \hat{\mathbf{G}}, \hat{\mathbf{H}}$	transformed flux vectors in ξ, η, ζ
l^i	ith left eigenvector
$\mathbf{N}$	cell face normal $[n_x, n_y, n_z]^T$
$\mathbf{Q}$	state vector of conserved variables
r	TVD limiter function argument
r^i	ith right eigenvector
R_n	nose radius
S	arc length along the wall
$\overleftarrow{S}$	backward cell distance
$\overrightarrow{S}$	forward cell distance
$\mathbf{U}$	velocity vector $[u,v,w]^T$
$\mathbf{W}$	contravariant velocity
a	characteristic vectors
$\overleftarrow{a}$	backward cell a
$\overrightarrow{\alpha}$	forward cell a
δ	entropy fix parameter
δ	entropy fix factor
λ	eigenvalue
σ	TVD limiter function
τ	transformed time

1. Introduction

The knowledge of the aerodynamic loads experienced by space vehicles at supersonic and hypersonic speeds is crucial for its successful design. These high speed configurations are invariably designed to have a blunt forebody due to heating rate considerations. The flow field of such blunt bodies is characterized by a strong detached bow shock and a thin shock layer with a subsonic pocket in the nose region. The computation of such a flow field is a challenging task.

As part of a program to compute such flows, a robust flow solver has been developed based on the solution of three dimensional time dependent Euler equations with ideal gas assumption. An explicit high resolution TVD scheme employing Roe's Riemann Solver has been formulated within the finite volume framework. The aim of this paper is to study, numerically, the effect of various entropy fixes and TVD limiters on accuracy, convergence and stability of computations for three dimensional blunt body high speed flows.

The Roe's Approximate Riemann Solver does not satisfy entropy condition at the sonic rarefactions and this results in expansion shocks. Anomalies for high Mach number flows besides entropy violation are also observed. Various formulations of entropy fixes are investigated in this paper.

The use of TVD limiters is essential in capturing strong blunt body shocks without wiggles. These limiters are however known to effect convergence. A study of various limiters on non-uniform grids has been undertaken by extending them to take into account cell center distances. These modifications dramatically improve convergence. Local time stepping and parallelization techniques are employed to accelerate convergence.

In each case, a full three dimensional axisymmetric grid is used with no symmetry boundary conditions.

2. Governing Equations

The non dimensionalized Euler equations cast in strong conservation law form in generalized body fitted coordinates can be written as

$$\frac{\partial \hat{\mathbf{Q}}}{\partial \tau} + \frac{\partial \hat{\mathbf{F}}}{\partial \xi} + \frac{\partial \hat{\mathbf{G}}}{\partial \eta} + \frac{\partial \hat{\mathbf{H}}}{\partial \zeta} = 0 \qquad (1)$$

For the transformation

$$\begin{aligned} \tau &= t \quad , \quad \xi = \xi(x,y,z), \\ \eta &= \eta(x,y,z) \quad , \quad \zeta = \zeta(x,y,z) \end{aligned} \qquad (2)$$

where

$$\hat{\mathbf{Q}} = \frac{1}{J}\begin{pmatrix} e \\ \rho \\ \rho u \\ \rho v \\ \rho w \end{pmatrix} \quad \hat{\mathbf{E}} = \frac{1}{J}\begin{pmatrix} (e+p)\mathbf{W} \\ \rho \mathbf{W} \\ \rho u \mathbf{W} + p\kappa_x \\ \rho v \mathbf{W} + p\kappa_y \\ \rho w \mathbf{W} + p\kappa_z \end{pmatrix} \qquad (3)$$

* Scientist, Senior Member AIAA

† Research Fellow

$Q = J\hat{Q}$ is the state vector of conserved variables and J is the Jacobian of the transformation. The contravariant velocity is given by $W = us, + v\kappa_y + w\kappa_z$. $\kappa = \xi, \eta, \zeta$ for the vectors $\hat{F}, \hat{G}, \hat{H}$ respectively. The Cartesian velocity components are u, v and w respectively and the velocity vector $U = u\,\hat{i} + v\,\hat{j} + w\,\hat{k}$ with $q^2 = U \cdot U$. The fluid density is p. The total energy per unit volume is $e = \rho I + \frac{1}{2}\rho q^2$ where I is the internal energy per unit mass of the gas. The pressure p is given by the equation of state $p = (\gamma - 1)\rho I$.

3. Numerical discretization

The semi-discrete conservation form of the equations is given by

$$\begin{aligned}(\overline{Q}_{i,j,k})_\tau &+ (\overline{F}_{i+\frac{1}{2},j,k} - \overline{F}_{i-\frac{1}{2},j,k}) \\ &+ (\overline{G}_{i,j+\frac{1}{2},k} - \overline{G}_{i,j-\frac{1}{2},k}) \\ &+ (\overline{H}_{i,j,k+\frac{1}{2}} - \overline{H}_{i,j,k-\frac{1}{2}}) = 0\end{aligned} \tag{4}$$

where overhead bars denote the numerically approximated vectors. A pseudo finite volume framework is obtained by the similarity relation $\overline{Q}_{i,j,k} = Q_{i,j,k}V_{i,j,k}$ for the volume $V_{i,j,k}$.

The cell volumes are computed by evaluating a combination of six tetrahedra that comprise it. The metrics κ_x/J, κ_y/J and κ_z/J for $\kappa = (\xi, \eta, \zeta)$ are related directly to the cell face normals n_x, n_y and n_z.

4. Numerical Scheme

The numerical scheme employed for the solution of the Euler equations is the upwind, TVD (MUSCL) formulation of Roe's Riemann Solver'.

We denote the cell face of interest as $m \pm \frac{1}{2}$ where $m = i, j$ or k for the calculation of fluxes F,G,H respectively. The numerical inviscid fluxes are represented collectively as $\overline{E}_{m+\frac{1}{2}}(Q, N)$. The local cell face normal is $N = n_x\hat{i} + n_y\hat{j} + n_z\hat{k}$.

5. Roe's Riemann Solver

The left state of the cell face of the state vector of conserved variables after the MUSCL preprocessing is Q^- and the state vector to the right of the cell face is Q^+. The interface enthalpy, $h = \gamma p/(\gamma - 1)\rho + q^2/2$ besides the density and velocity components are used for this purpose. The flux difference scheme, based on Roe's Riemann Solver[3] utilizes the following linearization at $m + \frac{1}{2}$, between the left and right states.

$$\begin{aligned}\chi &= \sqrt{\rho^+_{m+\frac{1}{2}}/\rho^-_{m+\frac{1}{2}}} \\ \rho_{m+\frac{1}{2}} &= \rho^-_{m+\frac{1}{2}}\chi \\ u_{m+\frac{1}{2}} &= (u^+_{m+\frac{1}{2}}\chi + u^-_{m+\frac{1}{2}})/(1+\chi) \\ v_{m+\frac{1}{2}} &= (v^+_{m+\frac{1}{2}}\chi + v^-_{m+\frac{1}{2}})/(1+\chi) \\ w_{m+\frac{1}{2}} &= (w^+_{m+\frac{1}{2}}\chi + w^-_{m+\frac{1}{2}})/(1+\chi) \\ h_{m+\frac{1}{2}} &= (h^+_{m+\frac{1}{2}}\chi + h^-_{m+\frac{1}{2}})/(1+\chi)\end{aligned} \tag{5}$$

where the acoustic speed at the interface is

$$c_{m+\frac{1}{2}} = \sqrt{[h_{m+\frac{1}{2}} - q^2_{m+\frac{1}{2}}/2](\gamma - 1)} \tag{6}$$

The Roe Linearization satisfies the conservation property for the cell face flux Jacobian

$$\overline{A}_{m+\frac{1}{2}} = \Delta\overline{E}_{m+\frac{1}{2}}/\Delta\overline{Q}_{m+\frac{1}{2}} \tag{7}$$

We obtain the eigenvalues and eigenvectors at the cell face by employing the Roe average values

$$\begin{aligned}\lambda^i_{m+\frac{1}{2}} &= \lambda^i_{m+\frac{1}{2}}(Q_{m+\frac{1}{2}}, N_{m+\frac{1}{2}}) \\ l^i_{m+\frac{1}{2}} &= l^i_{m+\frac{1}{2}}(Q_{m+\frac{1}{2}}, N_{m+\frac{1}{2}}) \\ r^i_{m+\frac{1}{2}} &= r^i_{m+\frac{1}{2}}(Q_{m+\frac{1}{2}}, N_{m+\frac{1}{2}})\end{aligned} \tag{8}$$

At every cell face we define the positive and negative components of the eigenvalues by

$$\lambda^{i\pm} = \frac{(\lambda^i_{m+\frac{1}{2}} \pm |\lambda^i_{m+\frac{1}{2}}|)}{2}, \qquad i = 1, \ldots, 5 \tag{9}$$

Roe's Riemann solver yields spurious non-physical phenomena such as expansion shocks at sonic rarefactions and has to be modified by added dissipation at these locations.

The model used for constructing the "entropy *fix*" to avoid these nonphysical solutions is discussed later in this paper. This circumvents the pitfalls of Roe's method.

The eigenvalues are given by

$$\begin{aligned}\lambda^1 &= W - c\sqrt{n_x^2 + n_y^2 + n_z^2} \\ \lambda^{2,3,4} &= \overline{W} \\ \lambda^5 &= \overline{W} + c\sqrt{n_x^2 + n_y^2 + n_z^2}\end{aligned} \tag{10}$$

where

$$\overline{W} = \frac{1}{J}W = U \cdot N \tag{11}$$

The numerical flux for the scheme, $\overline{E}_{m+\frac{1}{2}}$ is given by the general formulation

$$\begin{aligned}\overline{E}_{m+\frac{1}{2}} = &\frac{1}{2}[\,\overline{E}(Q^+_{m+\frac{1}{2}}, N_{m+\frac{1}{2}}) + \overline{E}(Q^-_{m+\frac{1}{2}}, N_{m+\frac{1}{2}})\,] \\ &-\frac{1}{2}[\,\sum_i |\lambda^i_{m+\frac{1}{2}}|\alpha^i_{m+\frac{1}{2}} r^i_{m+\frac{1}{2}}\,]\end{aligned} \tag{12}$$

where the charcteristic vector $\alpha^i_{m+\frac{1}{2}}$ is obtained as

$$\alpha^i_{m+\frac{1}{2}} = l^i_{m+\frac{1}{2}}(Q^+_{m+\frac{1}{2}} - Q^-_{m+\frac{1}{2}}) \tag{13}$$

6. TVD (MUSCL) formulation

The higher order MUSCL interpolation for the characteristic vectors is obtained as follows.

The following variables fcr state vector of characteristic variables are defined to obtain the left cell face state

vector of conserved variables $Q^-_{m+\frac{1}{2}}$ as derived later in this section

$$\begin{aligned} \overleftarrow{\alpha}^i_m &= l^i_m(\mathbf{Q}_m - \mathbf{Q}_{m-1}) \\ \overrightarrow{\alpha}^i_m &= l^i_m(\mathbf{Q}_{m+1} - \mathbf{Q}_m) \end{aligned} \tag{14}$$

We obtain the right cell face state vector of conserved variables $Q^+_{m+\frac{1}{2}}$ by defining

$$\begin{aligned} \overleftarrow{\alpha}^i_{m+1} &= l^i_{m+1}(\mathbf{Q}_{m+1} - \mathbf{Q}_m) \\ \overrightarrow{\alpha}^i_{m+1} &= l^i_{m+1}(\mathbf{Q}_{m+2} - \mathbf{Q}_{m+1}) \end{aligned} \tag{15}$$

where the ith left eigenvector at the cell m is given by

$$l^i_m = l^i(\mathbf{Q}_m, (\mathbf{N}_{m+\frac{1}{2}} + \mathbf{N}_{m-\frac{1}{2}})/2) \tag{16}$$

The ith right eigenvector at the cell m is given by

$$r^i_m = r^i(\mathbf{Q}_m, (\mathbf{N}_{m+\frac{1}{2}} + \mathbf{N}_{m-\frac{1}{2}})/2) \tag{17}$$

From the defintions above the **MUSCL** preprocessing yields the left and right state vectors of cell face $m+\frac{1}{2}$

$$\begin{aligned} \mathbf{Q}^-_{m+\frac{1}{2}} &= \mathbf{Q}_m + \sum_i \left(\frac{1+\phi}{4}\overrightarrow{\beta}^i_m + \frac{1-\phi}{4}\overleftarrow{\beta}^i_m\right) r^i_m \\ \mathbf{Q}^+_{m+\frac{1}{2}} &= \mathbf{Q}_{m+1} - \sum_i \left(\frac{1+\phi}{4}\overrightarrow{\beta}^i_{m+1} \right. \\ &\quad \left. + \frac{1-\phi}{4}\overleftarrow{\beta}^i_{m+1}\right) r^i_{m+1} \end{aligned} \tag{18}$$

The vectors $\overleftarrow{\beta}^i_m$ and $\overrightarrow{\beta}^i_m$ are obtained from the vectors $\overleftarrow{\alpha}^i_m$ and $\overrightarrow{\alpha}^i_m$ and the vectors $\overleftarrow{\beta}^i_{m+1}$ and $\overrightarrow{\beta}^i_{m+1}$ are obtained from the vectors $\overleftarrow{\alpha}^i_{m+1}$ and $\overrightarrow{\alpha}^i_{m+1}$ by using TVD limiters.

At maxima or minima the overall scheme reduces to first order. In the present study, the second order fully upwind formulation *i.e.* $\phi = -1$ has been employed throughout.

The interpolated values now represent the left and right states of Roe's Riemann Solver. We will refer to $Q^-_{m+\frac{1}{2}}$ and $\mathbf{Q}^+_{m+\frac{1}{2}}$ as Q_L and Q_R alternatively. Various limiters are available to determine the vectors $\overleftarrow{\beta}^i_m$ and $\overleftarrow{\beta}^i_{m+1}$. Note that $\overrightarrow{\beta}^i_m$ and $\overrightarrow{\beta}^i_{m+1}$ drop out for the upwind scheme.

7. TVD limiters

A large number of TVD limiters have been used to develop high resolution schemes[2] and have been studied for simple one dimensional and two dimensional problems. A detailed three dimensional numerical study of some of the popular limiters has been attempted by the authors in the present work. The sections to follow, describe various limiters formulated for a uniform mesh and the corresponding modifications, depending on cell distances, for a nonuniform mesh[8]. The limiters are generally defined in terms of the function

$$r = \overleftarrow{\alpha}^i_m / \overrightarrow{\alpha}^i_m \tag{19}$$

The nonuniformity of the mesh is taken into account by defining the cell center distances. The position vectors to the cell centroid are defined in terms of the vectors s. We define the following distances

$$\begin{aligned} \overleftarrow{S}_m &= |\mathbf{s}_m - \mathbf{s}_{m-1}| \\ \overrightarrow{S}_m &= |\mathbf{s}_{m+1} - \mathbf{s}_m| \\ \overleftarrow{S}_{m+1} &= |\mathbf{s}_{m+1} - \mathbf{s}_m| \\ \overrightarrow{S}_{m+1} &= |\mathbf{s}_{m+2} - \mathbf{s}_{m+1}| \end{aligned} \tag{20}$$

7.1 Chakravarthy-Osher limiter

This limiter is also called the minmod limiter. The formulation for the Chakravarthy-Osher limiter is given by the limiter function of the form[2]

$$\sigma(\hat{r}) = \text{minmod}(\hat{r}, \psi) \tag{21}$$

where the minmod function is given by

$$\begin{aligned} \text{minmod}[x, y] &= \text{sign}(x)\max\{0, \\ &\quad \min[|x|, y\,\text{sign}(x)]\} \end{aligned} \tag{22}$$

and the compression parameter ψ is

$$1 \le \psi \le \frac{3-\phi}{1-\phi} \tag{23}$$

We obtain the vectors in Eq. (18) using the minmod limiter as follows

$$\begin{aligned} \overleftarrow{\beta}^i_m &= \text{minmod}(\overleftarrow{\alpha}^i_m, \psi\overrightarrow{\alpha}^i_m) \\ \overleftarrow{\beta}^i_{m+1} &= \text{minmod}(\overrightarrow{\alpha}^i_{m+1}, \psi\overleftarrow{\alpha}^i_{m+1}) \end{aligned} \tag{24}$$

The corresponding formulation for a nonuniform mesh is as follows :

$$\begin{aligned} \overleftarrow{\beta}^i_m &= \text{minmod}((\overrightarrow{S}_m/\overleftarrow{S}_m)\overleftarrow{\alpha}^i_m, \psi\overrightarrow{\alpha}^i_m) \\ \overleftarrow{\beta}^i_{m+1} &= \text{minmod}((\overleftarrow{S}_{m+1}/\overrightarrow{S}_{m+1})\overrightarrow{\alpha}^i_{m+1}, \psi\overleftarrow{\alpha}^i_{m+1}) \end{aligned} \tag{25}$$

7.2 Roe Diffusive limiter

This limiter is the most diffusive of all the limiters studied by the authors and is obtained by setting the compression parameter ψ in Eq. (23) to 1. The formulation for this limiter then follows from the limiter described above.

7.3 van Albada limiter

The van Albada limiter is formally defined by the function

$$\sigma(\hat{r}) = \frac{\hat{r} + |\hat{r}|}{1 + \hat{r}^2} \tag{26}$$

We define the slopes $\Delta\alpha^i_m$ and $\Delta\alpha^i_{m+1}$ as

$$\begin{aligned}\Delta\alpha^i_m &= \text{sign}(\vec{\alpha}^i_m)\min(|\overleftarrow{\alpha}^i_m|, |\vec{\alpha}^i_m|)\\ \Delta\alpha^i_{m+1} &= \text{sign}(\overleftarrow{\alpha}^i_{m+1})\min(|\vec{\alpha}^i_{m+1}|, |\overleftarrow{\alpha}^i_{m+1}|)\end{aligned} \quad (27)$$

which are then treated by using the limiter function. The function defined for the ith characteristic vector is given by

$$\sigma^i_m = \frac{\overleftarrow{\alpha}^i_m \vec{\alpha}^i_m + |\alpha^i_m \alpha^i_m| + \epsilon}{(\overleftarrow{\alpha}^i_m)^2 + (\vec{\alpha}^i_m)^2 + \epsilon} \quad (28)$$

where ϵ is a small number which prevents division by zero and $0 \le \sigma^i_m \le 1$.

The nonuniformity of the mesh is treated by modifying the slope in **Eq.** (27)

$$\begin{aligned}\Delta\alpha^i_m &= \text{sign}(\vec{\alpha}^i_m)\min(|\frac{\vec{S}_m}{\overleftarrow{S}_m}\overleftarrow{\alpha}^i_m|, |\vec{\alpha}^i_m|)\\ \Delta\alpha^i_{m+1} &= \text{sign}(\overleftarrow{\alpha}^i_{m+1})\min(|\frac{\overleftarrow{S}_{m+1}}{\vec{S}_{m+1}}\vec{\alpha}^i_{m+1}|, |\overleftarrow{\alpha}^i_{m+1}|)\end{aligned} \quad (29)$$

The limiter function in **Eq. (28)** is modified as

$$\sigma^i_m = \frac{\left(\frac{\overleftarrow{\alpha}^i_m}{\overleftarrow{S}^i_m}\right)\left(\frac{\vec{\alpha}^i_m}{\vec{S}^i_m}\right) + \left|\left(\frac{\overleftarrow{\alpha}^i_m}{\overleftarrow{S}^i_m}\right)\left(\frac{\vec{\alpha}^i_m}{\vec{S}^i_m}\right)\right| + \epsilon}{\left(\frac{\overleftarrow{\alpha}^i_m}{\overleftarrow{S}^i_m}\right)^2 + \left(\frac{\vec{\alpha}^i_m}{\vec{S}^i_m}\right)^2 + \epsilon} \quad (30)$$

where the variable $\hat{r}$ for a nonuniform mesh can be defined as

$$\hat{r} = \frac{\left(\overleftarrow{\alpha}^i_m / \overleftarrow{S}^i_m\right)}{\left(\vec{\alpha}^i_m / \vec{S}^i_m\right)} \quad (31)$$

We then obtain the slope with limiters, **Eq. (18)**, by using the formulation for a uniform mesh given by **Eq. (27)** and **Eq. (28)** or for a nonuniform mesh given by **Eq. (29)** and **Eq. (30)**

$$\begin{aligned}\vec{\beta}^i_m &= \sigma^i_m \Delta\alpha^i_m\\ \overleftarrow{\beta}^i_{m+1} &= \sigma^i_{m+1}\Delta\alpha^i_{m+1}\end{aligned} \quad (32)$$

which reduces to zero at local maxima or minima.

7.4 van Leer limiter

The van Leer limiter is given by the function

$$\sigma(\hat{r}) = \frac{\hat{r} + |\hat{r}|}{1 + |\hat{r}|} \quad (33)$$

The limiter for the ith characteristic vector is defined by

$$\sigma^i_m = \frac{\overleftarrow{\alpha}^i_m \vec{\alpha}^i_m + |\overleftarrow{\alpha}^i_m \vec{\alpha}^i_m| + \epsilon}{(\vec{\alpha}^i_m)^2 + |\overleftarrow{\alpha}^i_m \vec{\alpha}^i_m| + \epsilon} \quad (34)$$

where ϵ is a small number which prevents division by zero as given for the van Albada limiter.

This limiter is modified for nonuniform meshes as

$$\sigma^i_m = \frac{\left(\frac{\overleftarrow{\alpha}^i_m}{\overleftarrow{S}^i_m}\right)\left(\frac{\vec{\alpha}^i_m}{\vec{S}^i_m}\right) + \left|\left(\frac{\overleftarrow{\alpha}^i_m}{\overleftarrow{S}^i_m}\right)\left(\frac{\vec{\alpha}^i_m}{\vec{S}^i_m}\right)\right| + \epsilon}{\left(\frac{\vec{\alpha}^i_m}{\vec{S}^i_m}\right)^2 + \left|\left(\frac{\overleftarrow{\alpha}^i_m}{\overleftarrow{S}^i_m}\right)\left(\frac{\vec{\alpha}^i_m}{\vec{S}^i_m}\right)\right| + \epsilon} \quad (35)$$

where the expression for **f** when considering a nonuniform mesh is given by **Eq. (31).**

The corrresponding limiter functions for uniform and nonuniform meshes is given by **Eq. (34)** and **Eq. (35)** respectively. The slopes are defined by **Eq.** (27) and **Eq.** (29) alternatively.

We then obtain the slope limited functions in **Eq. (18)** by the relation used in **Eq.** (32).

7.5 Roe Superbee limiter

The Superbee limiter is the most compressive of all the limiters mentioned in this study. The functional form of the limiter is given by

$$\sigma(\hat{r}) = \text{superbee}(\hat{r}, 1) \quad (36)$$

where we define the function superbee as

$$\text{superbee}(x, y) = \max[0, \min(2x, y), \min(x, 2y)] \quad (37)$$

We obtain the variable vectors in Eq. **(18)** using the superbee limiter as follows

$$\begin{aligned}\overleftarrow{\beta}^i_m &= \text{superbee}(\overleftarrow{\alpha}^i_m, \vec{\alpha}^i_m)\\ \overleftarrow{\beta}^i_{m+1} &= \text{superbee}(\vec{\alpha}^i_{m+1}, \overleftarrow{\alpha}^i_{m+1})\end{aligned} \quad (38)$$

The nonuniformity of the mesh is decided by the changing the above formulation as

$$\begin{aligned}\overleftarrow{\beta}^i_m &= \text{superbee}(\frac{\vec{S}_m}{\overleftarrow{S}_m}\overleftarrow{\alpha}^i_m, \vec{\alpha}^i_m)\\ \overleftarrow{\beta}^i_{m+1} &= \text{superbee}(\frac{\overleftarrow{S}_{m+1}}{S_{m+1}}\vec{\alpha}^i_{m+1}, \overleftarrow{\alpha}^i_{m+1})\end{aligned} \quad (39)$$

7.6 Davis limiter

The Davis limiter is defined by the function

$$\sigma(\hat{r}) = \text{minmod}(2\hat{r}, 1) \quad (40)$$

The minmod limiter is defined in Eq. (22).

The implementation for uniform meshes is

$$\begin{aligned} \overleftarrow{\beta}^i_m &= \text{minmod}(2\overleftarrow{\alpha}^i_m, \overrightarrow{\alpha}^i_m) \\ \overleftarrow{\beta}^i_{m+1} &= \text{minmod}(2\overrightarrow{\alpha}^i_{m+1}, \overleftarrow{\alpha}^i_{m+1}) \end{aligned} \tag{41}$$

The formulation for a nonuniform mesh is given by

$$\begin{aligned} \overleftarrow{\beta}^i_m &= \text{minmod}(2\frac{\overrightarrow{S}_m}{\overleftarrow{S}_m}\overleftarrow{\alpha}^i_m, \overrightarrow{\alpha}^i_m) \\ \overleftarrow{\beta}^i_{m+1} &= \text{minmod}(2\frac{\overleftarrow{S}_{m+1}}{\overrightarrow{S}_{m+1}}\overrightarrow{\alpha}^i_{m+1}, \overleftarrow{\alpha}^i_{m+1}) \end{aligned} \tag{42}$$

8. Entropy Fix

The main drawback in the Roe linearization inspite of its accuracy is the violation of entropy at sonic rarefactions. These are not the only problems faced by this method. Quirk[4] has illustrated various other pitfalls; the formation of Carbuncle shocks, strong odd-even coupling of pressure and density resulting in the breakdown of grid aligned planar shocks, negative internal energies, kinked mach stems and inability to resolve slow moving shocks. Furthermore, It has been noted that Harten's entropy fix and its variants invariably cure these when the fixes are also applied to the linear waves. The entropy corrections studied in the present work are that by Chakravarthy' and three variants of the basic Harten fix[5,6,7].

8.1 Chakravarthy entropy fix

In this formulation a correction is applied only at the sonic rarefactions ($\lambda^i(\mathbf{Q}_m, \mathbf{N}_{m+\frac{1}{2}}) < 0 < \lambda^i(\mathbf{Q}_{m+1}, \mathbf{N}_{m+\frac{1}{2}})$). This is given by correcting the eigenvalue spectrum at these points as follows

$$\begin{aligned} \lambda^{i\pm}_{m+\frac{1}{2}} &= \lambda^{i\pm}_{m+\frac{1}{2}} \\ &\pm \frac{(\lambda(\mathbf{Q}^i_{m+1}, \mathbf{N}_{m+\frac{1}{2}}) - \lambda(\mathbf{Q}^i_m, \mathbf{N}_{m+\frac{1}{2}}))}{4} \end{aligned} \tag{43}$$

where the latter term in brackets represent the added dissipation at sonic rarefactions.

8.2 Harten/Harten-Yee entropy fix

The general form of Harten's entropy fix is given by Harten[5]

$$|\lambda| = \begin{cases} |\lambda|, & \text{if } |\lambda| \geq \delta \\ (\lambda^2 + \delta^2)/(2\delta), & \text{if } |\lambda| < \delta \end{cases} \tag{44}$$

where $0.05 \leq 6 \leq 0.25$. Variants to the basic Harten's entropy fix have been developed depending on how 6 is specified.

A study by Yee[7] demonstrates that δ has to be modified for hypersonic flows as follows

$$\begin{aligned} \delta &= \delta^*[|\overline{\mathbf{W}}^\xi_{m+\frac{1}{2}}| + |\overline{\mathbf{W}}^\eta_{m+\frac{1}{2}}| + |\overline{\mathbf{W}}^\zeta_{m+\frac{1}{2}}| \\ &+ \frac{1}{3}c(|\nabla\xi| + |\nabla\eta| + |\nabla\zeta|)] \end{aligned} \tag{45}$$

wliere $\overline{\mathbf{W}}^\xi$, $\overline{\mathbf{W}}^\eta$ and $\overline{\mathbf{W}}^\zeta$ are the contravariant velocities in ξ, η and ζ directions respectively, and $0.05 \leq 6' \leq 0.25$.

8.3 Harten – Hyman variant of Harten's fix

The following entropy fix due to Harten and Hyman[6] relates the entropy fix to average state between the left and right states of the interface. The parameter 6 Eq. (44) is given by

$$\begin{aligned} \delta = \max[0, &\{\lambda^i(Q_L, Q_R) - \lambda^i(Q_L, \mathbf{Q}(\theta))\}, \\ &\{\lambda^i(\mathbf{Q}(\theta), Q_R) - \lambda^i(Q_L, \mathbf{Q}_R)\}] \end{aligned} \tag{46}$$

where. $\lambda^i(a, b)$ is the eigenvalue obtained from the Roe-Averaged value of the left and right states (a,b). In the above equation the vector $\mathbf{Q}(\theta)$ is given by

$$\mathbf{Q}(\theta) = {}_{QL} + \theta(\mathbf{Q}_R - \mathbf{Q}_L)$$

for $0 \leq 8 \leq 1$. A constant θ of 0.5 has been used in the present study.

9. Boundary Conditions

The following boundary conditions have been used :

9.1 Inflow/Outflow Boundary

Freestream conditions have been imposed at the inflow boundary. A two cell specification at the inflow boundary takes care of the High Resolution scheme. At the outflow a first order extrapolation in the streamwise–ξ direction is implemented as

$$\frac{\partial^2 \mathbf{Q}}{\partial \xi^2} = 0 \tag{47}$$

9.2 Wall Boundary

We obtain the right state at the wall, denoted by the R-subscipted values, by extrapolating from the interior of the flow field. The wall boundary conditions are imposed by the exact solution of the one sided Riemann problem.

$$\begin{aligned} (p/\rho^\gamma)_W &= (p/\rho^\gamma)_R \\ (u - \frac{2}{\gamma - 1}{}_W c) &= (u - \frac{2}{\gamma - 1}c)_R \end{aligned} \tag{48}$$

where the subscript W represents the wall conditions. Since, the Euler wall boundary condition implies zero normal velocity the one dimensional solution procedure given above results in $u_W = 0$.

From the two equations above, we get

$$p_W = p_R(1 - \frac{\gamma - 1}{2}\frac{u_R}{c_R})^{2\gamma/(\gamma-1)} \qquad (49)$$

Since, the scheme is second order accurate, we create a ghost cell next to the wall, values for which is obtained by reflection.

9.3 Grid singularity treatment

The three dimensional axisymmetric grid is generated by rotating a two dimensional grid by 360°. This generates an axial singularity where the surface collapses into a line. This is treated in the present study by merging all the pyramid cells adjoining the singular line into a larger cell which looks like a frustrum of a cone with an outer polyhedral surface. The flux balance across this cell is treated specially by considering the outgoing flux across all the polyhedral surfaces and thus circumventing the problem of considering the physical nature of flux across a singularity.

10. Test Cases and Grid generation

The two test cases employed for the study of supersonic and hypersonic blunt body flows are :

1. Supersonic flow over a hemisphere-cylinder at a freestream Mach number of 2.94 and zero angle of attack (Case 1).
2. Hypersonic flow over a hemisphere-cone (semi cone angle of 15") at a freestream Mach number of 10.6 and an angle of attack of 15" (Case 2).

An algebraical grid generator with uniform cell spacing normal to the wall and streamwise stretching along the cylinder/cone has been used (Fig. 1 and Fig. 2). The three dimensional axisymmetric grid was generated by rotating the two dimensional grid by 360" with uniform spacing in the circumferential direction .

The grid defintion in both Case 1. and Case 2 was (25x19x20) in ξ, η and ζ. These are the streamwise direction, direction normal to the wall and crosswise direction. It will be shown later that this crude grid definition did not effect shock resolution.

11. Parallelization technique

The computer code was implemented on the Flosolver MK3, a parallel machine based on the Intel i860 chip. The Flosolver has a master processor called the Host which takes care of the i/o and slave processors, designated as PE, which in conjunction with the Host are used for number crunching (Fig. 3). A maximum of 16 simultaneous processors can be used (6-12 MFLOPS per processor). The procedure used to effect computation is domain decomposition along the streamwise-ξ direction on a 4 node implementation. An overlap of two cells between the four processors is provided to facilitate the second order implementation of the scheme.

12. Results and Discussions

This section is divided into four subsections. First, the effect of using nonlinear interpolation in TVD limiters is considered. Next, the comparative study of scaled TVD limiters and entropy fixes is shown. Finally, the results of the computed flowfield for Case 1 and Case 2 are presented and discussed.

12.1 Nonlinear interpolation

Case 2 (hypersonic flow) has been chosen for this study. The entropy fix due to Harten–Yee and the Roe Diffusive limiter has been studied in this section. The convergence histories of scaled and unscaled limiters is shown in Fig. 4. The inclusion of mesh spacing in the formulation of TVD limiters results in a dramatic improvement in the convergence characteristics.

All the results presented below involve the use of limiters with nonlinear interpolation involving mesh spacing.

12.2 Comparative study of Limiters

The various formulation of limiters are tested on the Case 2 (hypersonic flow) with entropy fix due to Harten-Yee and their performance compared in terms of convergence in Fig. 5. It may be observed that the Roe Diffusive limiter provides the best convergence and the Davis limiter the worst.

12.3 Comparative Study of Entropy Fixes

The performance of three entropy fixes – Chakravarthy, Harten and Harten-Hyman is compared in terms of convergence characteristics in Fig. 6 for Case 1. An improved convergence is obtained for Harten's fix where 6 in Eq. (44) was set at 0.125. The performance of tlie other two fixes is similar. It was observed that the choice of the entropy fix does not have any significant effect on the accuracy of the above computations.

The fixes mentioned above however do not provide proper convergence characteristics for hypersonic flow computations (Case 2). The Harten-Yee modification of the basic Harten's entropy fix has been found to be quite robust for hypersonic Row computations. The value of δ^*, Eq. (45), used in these computations was 0.15.

The entropy fixes mentioned above are useful for supersonic flows. However, the Harten-Hyman fix is computationally expensive. Only the Harten-Yee extension is reliable in hypersonic cases where the others fail. It is found that most of the shortcomings of Roe's scheme for blunt body flow computations can be overcome by the appropriate choice of the entropy fix suited for a particular Mach number range.

12.4 Computed flow field

All the flow field results presented below have the Roe

Diffusive limiter for the High Resolution scheme. The entropy fix is the Harten's fix for the Case 1 and the Harten-Yee extension of the Harten's fix for Case 2. The accuracy is found to be independent of the choice of limiter, although convergence is affected by them.

The density contours for Case 1 are shown in Fig. 7. The shock is resolved accurately even on the crude grid used. The computed pressure distribution over the body is shown in Fig. 8 and compares well with the computation due to Viviand *et. al.* [9].

The hypersonic Case 2 is studied next. The pressure contours are given in Fig. 9. The computed coefficient of pressure on the body is shown in Fig. 10. The comparison to this figure is made with the experimental study by Cleary[10] and computational work by Riedelbauch *et.* al. [11]. The Mach number contours for the same case is shown in Fig. 11. The symmetry about the pitch plane is demonstrated in Fig. 12 by the cross plane density contours.

Concluding Remarks

A Flow Solver for the solution of three dimensional Euler Equations to compute supersonic and hypersonic blunt body flows has been developed based on an unpwind TVD (MUSCL) formulation of the Roe's method. A compatible wall boundary condition procedure with a special treatment of the singularity line for axisymmetric blunt bodies enhances the robustness of the Flow Solver.

A comparative study of various limiters and entropy fixes has been done to identify the most appropriate combination of the limiter and the entropy fix for the Mach number range of interest. The choice of limiters has an important effect on the convergence characteristics of the flow computations. Furthermore, the robustness of the Solver is dictated by the appropriate choice of limiter and entropy fix. The inclusion of cell distances to account for mesh nonuniformity in the limiter formulation shows a dramatic improvement in the convergence characteristics. The present study demonstrates that the Roe diffusive limiter with Harten/Harten-Yee entropy fix provides the best convergence. Excellent results at supersonic and hypersonic Mach numbers have been obtained with no deficiencies associated with Roe's method for this combination of limiter and entropy fix in blunt body computations. Local Time Stepping and the Parallelization technique have enhanced convergence in terms of effective wall clock times.

Acknowledgements

The present study was carried out in response to a request from DRDL, Iiyderabad. We thank Dr. T.S. Prahlad, Coordinator, Aerodynamics Panel, for making this study possible through an AR&DB Project No. CF-1-121. Many useful discussions with Prof. S.M. Deshpande and Dr. S.S Desai are acknowledged with thanks. Thanks are due to Dr. U.N. Sinha and his team at the FLOSOLVER Laboratory for their initial help in the parallelization of the code and usage of the FLOSOLVER machine.

References

[1] Chakravarthy, S.R., High resolution upwind formulations for the Navier-Stokes equations, VKI Lecture Series 1988-05, computational Fluid Dynamics, March 7–11, (1988).

[2] Sweby, P.K., High Resolution Schemes Using Flux Limiters for Hyperbolic Conservation Laws, SIAM J. Num. Ana. 21,995. (1984).

[3] Roe, P.L., Approximate Riemann Solvers, Parameter Vectors, and Difference Schemes, Journal of Computational Physics, Vol. 43, pp. 357-372, (1981).

[4] Quirk, J.J., A contribution to the Great Riemann Solver Debate, NASA Contractor Report 191409, ICASE Report No. 92-64, November 1992.

[5] Harten, A., On a Class of High Resolution Total-Variation-Stable Finite Difference Schemes, SIAM J. Num. Ana., Vol. 21, pp. 1-23, (1984).

[6] Harten, A. and Hyman, J.M., A Self-Adjusting Grid for the Computation of Weak Solutions of hyperbolic Conservation Laws, Journal of Computational Physics, Vol. 50, pp. 235-269 (1983).

[7] Yee H.C., A Class of High-Resolution Explicit and Implicit Shock-Capturing Method, NASA Technical Memorandum 101088, Feb. 1989.

[8] Turkel E., Accuracy of schemes with Nonuniform Meshes for Compressible Flows, ICASE Report 85-43, (1985).

[9] Viviand, H. and Ghazzi, W., Numerical solution of the compressible Navier-Stokes equations at high Reynolds number with applications to the blunt body problem, Lecture notes in Physics, Vol. 59, (1976).

[10] Cleary, J.W., An experimental and theoretical investigation of the pressure distribution and flow fields of blunted cones at hypersonic Mach numbers, NASA TN D-2969, (1965).

[11] Riedelbauch, S. and Müller, B., The Simulation of Three-Dimensional Viscous Supersonic Flow Past Blunt Bodies with a Hybrid Implicit/Explicit Finite-Difference Method, DFVLR-FB 87-32, (1987).

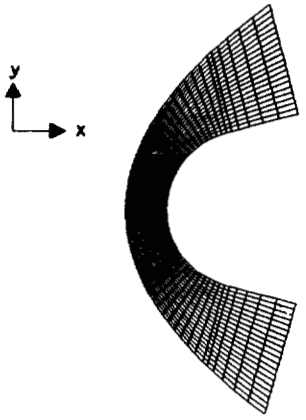

Fig. 1. Pitch plane grid.

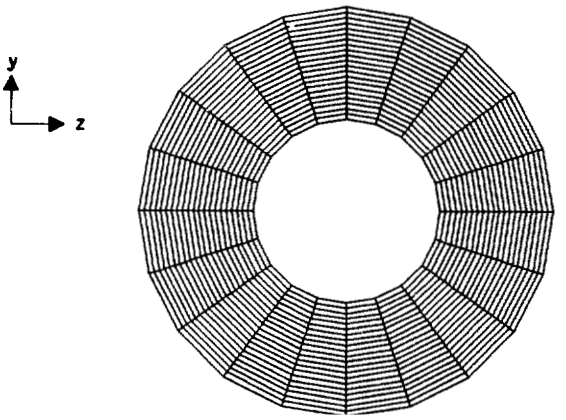

Fig. 2. Cross plane grid.

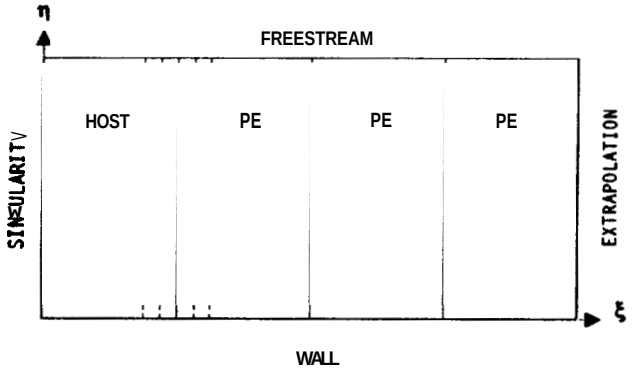

Fig. 3. Domain decomposition on the parallel computer, FLOSOLVER.

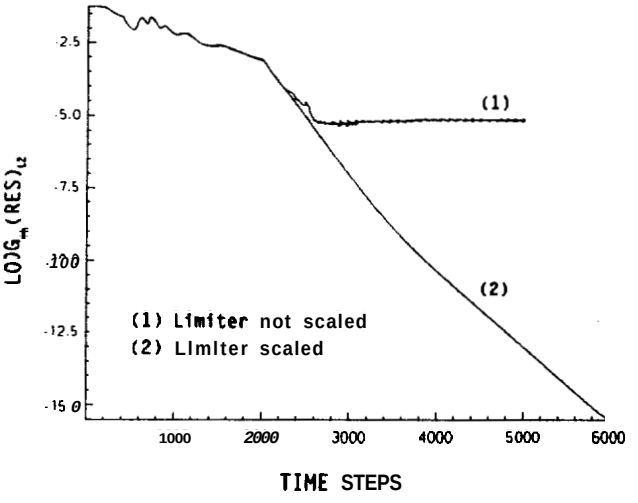

Fig. 4. Effect of nonlinear interpolation on limiters for Case 2.

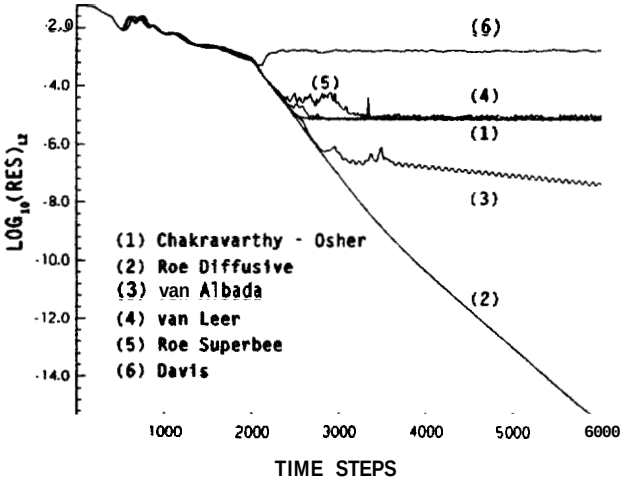

Fig. 5. Comparison of various TVD Limiters for Case 2.

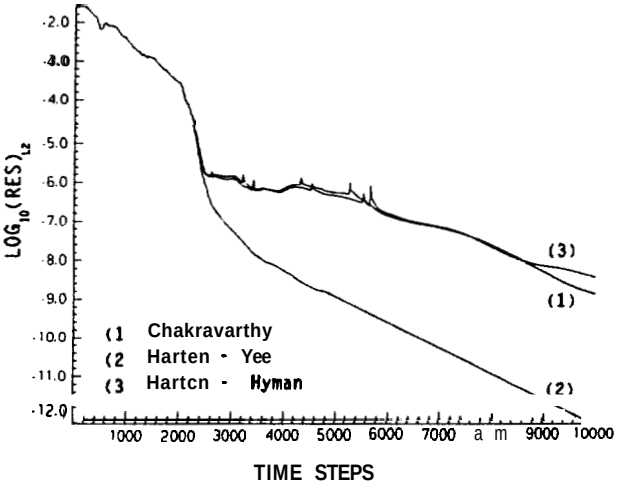

Fig. 6. Comparison of various Entropy Fixes for Case 1.

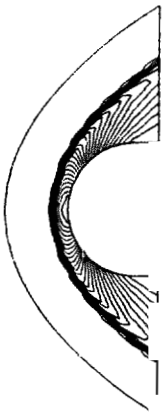

Fig. 7. Density contours in the pitch plane for Case 1.

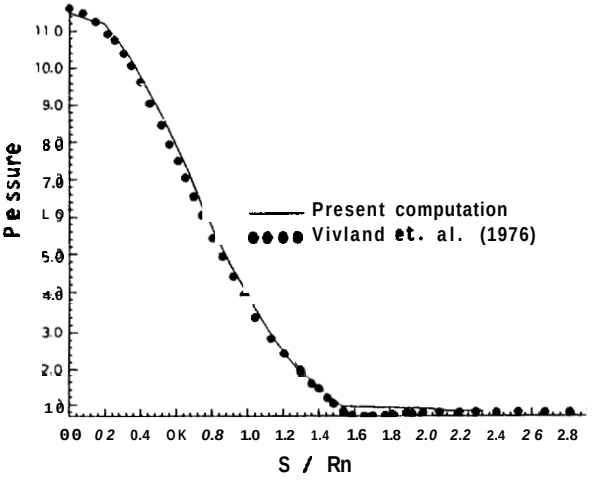

Fig. 8. Pressure distribution along the wall for Case 1.

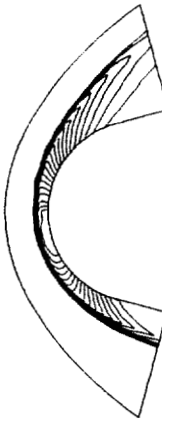

Fig. 9. Pressure contours in the pitch plane for Case 2.

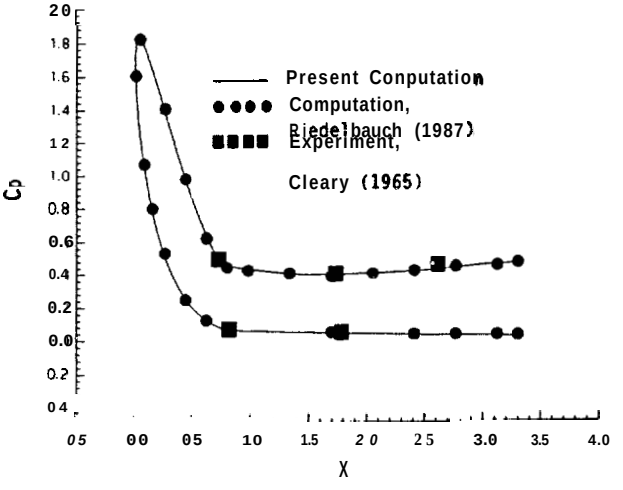

Fig. 10. Pressure distribution along the wall for Case 2.

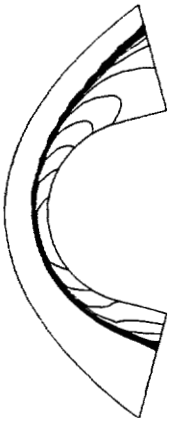

Fig. 11. Mach number contours in the pitch plane for Case 2.

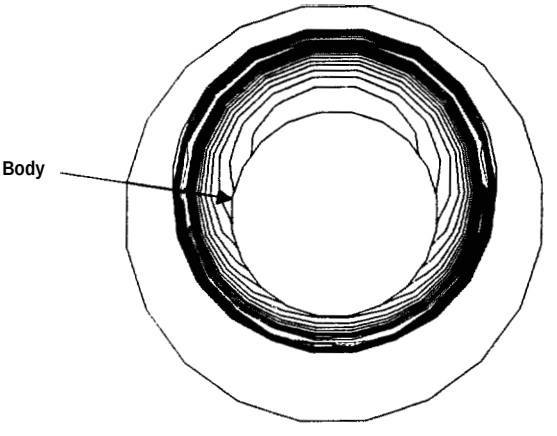

Fig. 12. density contours in the cross plane for Case 2.

AIAA-94-1875-CP

SOME ASPECTS OF THREE DIMENSIONAL SUPERSONIC/HYPERSONIC INVISCID BLUNT BODY FLOW COMPUTATIONS EMPLOYING HIGH RESOLUTION TVD SCHEMES BASED ON ROE'S RIEMANN SOLVER

S. K. Saxena * and K. Ravi †

Computational and Theoretical Fluid Dynamics Division
National Aerospace Laboratories
Bangalore, India

Abstract

This paper discusses some aspects of three dimensional supersonic and hypersonic inviscid blunt body flow computations. The method is based on the solution of the Euler equations employing an explicit, upwind TVD (MUSCL) formulation of the Roe Riemann Solver within the cell centered finite volume approach. A comparative study of various limiters and entropy fixes is carried out to identify the most appropriate combination. The effect of using cell spacing in the TVD extrapolations is highlighted. Local time stepping and code parallelization has been employed to accelerate convergence in terms of effective wall clock times.

Nomenclature

$\mathbf{A}$	flux Jacobian
C_p	pressure coefficient
$\hat{\mathbf{E}}$	transformed flux vector
$\hat{\mathbf{F}}, \hat{\mathbf{G}}, \hat{\mathbf{H}}$	transformed flux vectors in ξ, η, ζ
l^i	ith left eigenvector
$\mathbf{N}$	cell face normal $[n_x, n_y, n_z]^T$
$\mathbf{Q}$	state vector of conserved variables
r	TVD limiter function argument
r^i	ith right eigenvector
R_n	nose radius
S	arc length along the wall
$\overleftarrow{S}$	backward cell distance
$\overrightarrow{S}$	forward cell distance
$\mathbf{U}$	velocity vector $[u,v,w]^T$
$\mathbf{W}$	contravariant velocity
a	characteristic vectors
$\overleftarrow{a}$	backward cell a
$\overrightarrow{\alpha}$	forward cell a
δ	entropy fix parameter
δ	entropy fix factor
λ	eigenvalue
σ	TVD limiter function
τ	transformed time

1. Introduction

The knowledge of the aerodynamic loads experienced by space vehicles at supersonic and hypersonic speeds is crucial for its successful design. These high speed configurations are invariably designed to have a blunt forebody due to heating rate considerations. The flow field of such blunt bodies is characterized by a strong detached bow shock and a thin shock layer with a subsonic pocket in the nose region. The computation of such a flow field is a challenging task.

As part of a program to compute such flows, a robust flow solver has been developed based on the solution of three dimensional time dependent Euler equations with ideal gas assumption. An explicit high resolution TVD scheme employing Roe's Riemann Solver has been formulated within the finite volume framework. The aim of this paper is to study, numerically, the effect of various entropy fixes and TVD limiters on accuracy, convergence and stability of computations for three dimensional blunt body high speed flows.

The Roe's Approximate Riemann Solver does not satisfy entropy condition at the sonic rarefactions and this results in expansion shocks. Anomalies for high Mach number flows besides entropy violation are also observed. Various formulations of entropy fixes are investigated in this paper.

The use of TVD limiters is essential in capturing strong blunt body shocks without wiggles. These limiters are however known to effect convergence. A study of various limiters on non-uniform grids has been undertaken by extending them to take into account cell center distances. These modifications dramatically improve convergence. Local time stepping and parallelization techniques are employed to accelerate convergence.

In each case, a full three dimensional axisymmetric grid is used with no symmetry boundary conditions.

2. Governing Equations

The non dimensionalized Euler equations cast in strong conservation law form in generalized body fitted coordinates can be written as

$$\frac{\partial \hat{\mathbf{Q}}}{\partial \tau} + \frac{\partial \hat{\mathbf{F}}}{\partial \xi} + \frac{\partial \hat{\mathbf{G}}}{\partial \eta} + \frac{\partial \hat{\mathbf{H}}}{\partial \zeta} = 0 \qquad (1)$$

For the transformation

$$\begin{aligned} \tau &= t \quad , \quad \xi = \xi(x,y,z), \\ \eta &= \eta(x,y,z) \quad , \quad \zeta = \zeta(x,y,z) \end{aligned} \qquad (2)$$

where

$$\hat{\mathbf{Q}} = \frac{1}{J}\begin{pmatrix} e \\ \rho \\ \rho u \\ \rho v \\ \rho w \end{pmatrix} \quad \hat{\mathbf{E}} = \frac{1}{J}\begin{pmatrix} (e+p)\mathbf{W} \\ \rho \mathbf{W} \\ \rho u \mathbf{W} + p\kappa_x \\ \rho v \mathbf{W} + p\kappa_y \\ \rho w \mathbf{W} + p\kappa_z \end{pmatrix} \qquad (3)$$

* Scientist, Senior Member AIAA

† Research Fellow